A hypermorphic *Nfkbid* allele represents an *Idd7* locus gene contributing to impaired thymic deletion of autoreactive diabetogenic CD8$^+$ T-cells in NOD mice.[1,2]

Maximiliano Presa[*], Jeremy J. Racine[*], Deanna J Lamont[*], Jennifer Dwyer[*], Jeremy Ratiu[*], Vishal Kumar Sarsani[*], Yi-Guang Chen[†], Aron Geurts[†], Ingo Schmitz[‡§], Timothy Stearns[*], Jennifer Allocco[*], Harold D. Chapman[*], and David V. Serreze[*]

[*] The Jackson Laboratory, Bar Harbor, Maine USA.

[†] Medical College of Wisconsin, Milwaukee, Wisconsin USA

[‡] Systems-Oriented Immunology and Inflammation Research Group, Helmholtz Centre for Infection Research, Inhoffenstraße 7, 38124 Braunschweig

[§] Institute of Molecular and Clinical Immunology, Otto-von-Guericke University

Running Title: *Nfkbid* contributes to *Idd7*-control of negative selection.

Correspondence:

Dr. David Serreze, PhD

The Jackson Laboratory

600 Main St.

Bar Harbor, Maine 04609

ORCID: 0000-0001-7614-5925

dave.serreze@jax.org

(207) 288-6403

Abstract: 234/250 words

Text: 5786 words

Abstract:

In both NOD mice and humans the development of type 1 diabetes (T1D) is dependent at least in part on autoreactive $CD8^+$ T-cells recognizing pancreatic ß-cell peptides presented by often quite common MHC class I variants. Studies in NOD mice previously revealed the common K^d and/or D^b class I molecules expressed by this strain acquire an aberrant ability to mediate pathogenic CD8 T-cell responses through interactions with T1D susceptibility (*Idd*) genes outside the MHC. A gene(s) mapping to the *Idd7* locus on proximal Chromosome 7 was previously shown to be an important contributor to the failure of the common class I molecules expressed by NOD mice to mediate the normal thymic negative selection of diabetogenic $CD8^+$ T-cells. Using an inducible model of thymic negative selection and mRNA transcript analyses we initially identified an elevated *Nfkbid* expression variant as a strong candidate for an NOD *Idd7* region gene contributing to impaired thymic deletion of diabetogenic $CD8^+$ T-cells. CRISPR/Cas9-mediated genetic attenuation of *Nfkbid* expression in NOD mice resulted in improved negative selection of autoreactive diabetogenic AI4 and NY8.3 $CD8^+$ T-cells. These results indicated allelic variants of *Nfkbid* represent an *Idd7* gene contributing to the efficiency of intrathymic diabetogenic $CD8^+$ T-cell deletion. However, while enhancing thymic deletion of pathogenic $CD8^+$ T-cells, ablation of *NFkbid* expression surprisingly accelerated T1D onset in NOD mice likely by eliciting decreases in both regulatory T- and B-lymphocytes (Tregs/Bregs) mediating peripheral immunosuppressive effects.

45 **Introduction:**

46 In both the NOD mouse model and in humans, type 1 diabetes (T1D) results from the
47 autoimmune destruction of insulin-producing pancreatic β-cells mediated by the combined
48 activity of $CD4^+$ and $CD8^+$ T-cells as well as B-lymphocytes (1). T1D is highly polygenic in
49 nature, as more than 50 loci have been associated with disease susceptibility or resistance in both
50 humans and NOD mice (2, 3). However, while its complete pathogenic etiology remains
51 unsolved there is a wide acceptance that disease develops as a consequence of interactions
52 between T1D susceptibility (*Idd*) genes resulting in breakdowns in mechanisms controlling
53 induction of immunological tolerance to self-proteins (4, 5). Some *Idd* genes appear to contribute
54 to defects in central tolerance induction mechanisms that normally represent a first checkpoint
55 engendering the thymic deletion of autoreactive $CD4^+$ and $CD8^+$ T-cells during early stages of
56 their development (6-8). However, even in healthy individuals, some autoreactive T-cells escape
57 central tolerance mechanisms (9). Such autoreactive effectors are normally prevented from
58 mediating pathogenic effects by a second checkpoint, provided by multiple mechanisms of
59 peripheral tolerance induction, with significant evidence for some of these processes also being
60 disrupted by various *Idd* genes (5).

61 In the thymus, double positive (DP, $CD4^+CD8^+$) immature thymocytes are able to
62 recognize self-peptide-MHC complexes displayed on antigen presenting cells (APC, thymic
63 epithelial cells, dendritic cells (DC) or macrophages) through interactions with clonally
64 distributed T-cell receptor (TCR) molecules (10). The strength of TCR signaling resulting from
65 the trimolecular complex interaction, dictates the fate of immature DP thymocytes (9, 10). DP
66 thymocytes undergoing high avidity interactions with self-peptide-MHC complexes are normally
67 deleted by apoptosis or diverted to a regulatory T-cell lineage (Tregs, $CD4^+Foxp3^+$) (9).

68 Deficiencies in this process strongly contribute to the survival and presence in the periphery of
69 potentially autoreactive T-cells or inadequacies in self-antigen specific Tregs (5). Both in
70 humans and NOD mice, the defects in central tolerance can be exerted at three levels: reduced
71 presentation of self-antigen in thymus; defects in post-TCR engagement signaling events; and
72 variability in the basal or induced expression level of molecules controlling the final pro-/anti-
73 apoptotic balance (4, 5). Several *Idd* genes and loci have been identified as contributing to such
74 central tolerance induction defects (4, 5). Among these are MHC haplotypes long known to
75 provide the primary T1D genetic risk factor (11). Within the MHC, certain unusual class II
76 molecules play an important role in the pathogenesis of T1D by allowing the development and
77 functional activation of autoreactive $CD4^+$ T-cells (12). However, MHC class II expression is
78 largely restricted to thymic epithelial cells and hematopoietically derived APC (10, 13). Thus,
79 while class II restricted autoreactive $CD4^+$ T-cells clearly play a critical role in T1D
80 development, they cannot do so by directly engaging insulin producing pancreatic β cells (14).
81 Conversely, like most other tissues, pancreatic β cells do express MHC class I molecules. Hence,
82 due to an ability to directly engage and destroy pancreatic β cells, MHC class I restricted
83 autoreactive $CD8^+$ T-cells are likely the ultimate mediators of T1D development in both humans
84 and NOD mice (14, 15). Epidemiological studies have shown that in addition to class II effects,
85 particular HLA class I variants provide an independent T1D risk factor in humans (16, 17).
86 Interestingly, this includes some quite common MHC class I variants that in both humans and
87 NOD mice only acquire an aberrant ability to contribute to T1D when expressed in the context of
88 other *Idd* genes.

89 Previous studies found interactive contributions from some polymorphic *Idd* genes
90 outside of the MHC determine the extent to which particular class I molecules can allow the

development and functional activation of diabetogenic $CD8^+$ T-cells. This was initially demonstrated by congenically transferring a transgenic TCR (Vα8/Vβ2) from the $H2^{g7}$ class I restricted diabetogenic $CD8^+$ T-cell clone AI4 from a NOD genetic background strain (NOD-AI4) to a T1D resistant C57BL/6-stock congenic for the $H2^{g7}$ haplotype (B6.$H2^{g7}$). Autoreactive AI4 TCR transgenic T-cells were deleted to a significantly greater extent at the DP stage of thymic development in B6.$H2^{g7}$ than NOD mice (7). This result indicated non-MHC genes allelically differing in NOD and B6 background mice regulate the extent to which autoreactive diabetogenic $CD8^+$ T-cells undergo thymic deletion. Such non-MHC genes controlling differing thymic negative selection efficiency in NOD and B6 background mice were also found to function in a T-cell intrinsic manner (7). Subsequent linkage analyses and congenic strain evaluation identified a region on proximal Chromosome (Chr.) 7 to which the *Idd7* locus had been previously mapped *(18, 19)*, as containing a gene strongly contributing to the differential thymic deletion efficiency of diabetogenic AI4 $CD8^+$ T-cells in NOD and B6.$H2^{g7}$ mice (8).

In this study we identify *Nfkbid* as a likely *Idd7* region gene regulating the efficiency of diabetogenic CD8 T-cells thymic negative selection. *Nfkbid* (aka IκBNS) is a family member of the non-conventional IkB modulators of the transcription factor NF-κB (20). Depending on cell type and physiological context *Nfkbid* can either positively or negatively modulate NFkB activity (20). *Nfkbid* was first discovered as a gene expressed in thymocytes undergoing negative selection upon antigen specific TCR stimulation (21). Curiously, genetic ablation of *Nfkbid* in B6 background mice did not elicit any alteration in thymocyte subset distribution or any overt signs of autoimmunity (22). Using TCR transgenic mouse models to analyze antigen specific thymic negative selection, we show in this report that a higher expression variant of *Nfkbid* in NOD than B6 mice contributes to diminished negative selection in the former strain of both the AI4 and

114 NY8.3 MHC class I restricted autoreactive diabetogenic $CD8^+$ T-cell clonotypes. While genetic
115 attenuation of *Nfkbid* expression to levels similar to that in B6 background mice results in
116 improved thymic deletion of pathogenic $CD8^+$ T-cells, total ablation of this gene also diminishes
117 levels of peripheral immunoregulatory T- and B-lymphocytes (Tregs, Bregs) resulting in
118 accelerated T1D development in NOD mice.
119
120

121 **Materials and Methods**

122 *Mouse strains*

123 NOD/ShiLtDvs (NOD), B6.NOD-(D17Mit21-D17Mit10)/LtJ (B6.$H2^{g7}$) and NOD.Cg-
124 $Prkdc^{scid}$ Emv30b/Dvs (NOD.*scid*) mice are maintained in a specific pathogen free research
125 colony at The Jackson Laboratory. NOD.*Foxp3-eGFP* knockin mice, carrying the reporter
126 construct $Foxp3^{tm2(eGFP)-Tch}$ were previously described (23, 24). NOD mice carrying a transgenic
127 TCR (Vα8.3, Vβ2) derived from the AI4 diabetogenic $CD8^+$ T-cell clone (NOD-AI4) have also
128 been previously described (25). Previously generated NOD.LCMV mice transgenically express a
129 TCR (Vα2/Vβ8) from a $CD8^+$ T-cell clone recognizing the H2-D^b restricted gp33 peptide
130 (KAVYNFATM) derived from Lymphocytic Choriomeningitis Virus (LCMV) (26, 27). An
131 NOD stock transgenically expressing the TCR derived from the H2-K^d restricted diabetogenic
132 NY8.3 $CD8^+$ T-cell clone (28) (here designated NOD.NY8.3) were acquired from the type 1
133 diabetes resource (http://type1diabetes.jax.org/) and maintained in an heterozygous state. An
134 NOD stock congenic for a segment of B6-derived Chr. 7 delineated by the flanking markers Gpi^b
135 and *D7Mit346* (29), designated as NOD.$Ch7^{B6}$FL was used to introduce the interval into NOD-
136 AI4 mice (8).

137

138 *Congenic truncation analysis*

139 The NOD.$Ch7^{B6}$FL-AI4 stock was intercrossed with NOD-AI4. Resultant F1 progeny
140 were intercrossed and all F2 offspring were analyzed for recombination events in the Chr. 7
141 congenic region delineated by the flanking markers Gpi^b (34.2 Mb) and *D7Mit346* (58.7 Mb).
142 Genomic tail DNA samples were screened for the microsatellite markers *D7MIT267*, *D7MIT117,*
143 *D7MIT155, $Gpi1^b$, D7MIT79, D7MIT225, D7MIT78, D7MIT247, D7MIT270, D7MIT230,* and

144 *D7mit346* by PCR. Identified recombinant mice were backcrossed with NOD-AI4 and then
145 intercrossed to generate progeny homozygous for the sub-congenic regions. The homozygous
146 state for each congenic line generated was verified by PCR analyses of the markers listed above.
147
148 *Generation of NOD Nfkbid deficient mice*
149 CRISPR/Cas9 technology was utilized to directly ablate the *Nfkbid* gene in NOD mice
150 (NOD-*Nfkbid*$^{-/-}$). NOD/ShiLtDvs embryos were intra-cytoplasmic microinjected with 3 pl of a
151 solution containing Cas9 mRNA and single guide RNA (sgRNA) at respective concentrations of
152 100 ng/µl and 50 ng/µl. The sgRNA sequence (5'-AGGCCCATTTCCCCTGGTGA-3') was
153 designed to delete the transcriptional start site of *Nfkbid* in exon 3. Genomic tail DNA was
154 screened by targeted Sanger sequencing: the genomic region around exon 3 was amplified by
155 PCR with primers Nfkbid-KO-F1 (5'-TGCTTGAGATCCAGTAG-3') and Nfkbid-KO-R1 (5'-
156 CCCTGACATCTCAGAATA-3'), the resulting PCR product was purified and sequenced using
157 an ABI 3730 DNA analyzer (Applied Biosystems). Analyses of Sanger sequencing data was
158 done using the software Poly Peak Parser (30) which allows identification of the different alleles
159 present in heterozygous mutant mice. During the screening of N1 mutants we identified an allele
160 characterized by an 8 nt deletion and an insertion of 154 nt originated by copy and inversion of a
161 DNA segment from *Nfkbid* exon 2. This produced a major disruption of the *Nfkbid* gene and
162 deletion of the transcription start site (Supplementary Fig. 1). N1F1 NOD-*Nfkbid*$^{+/-}$ mutant mice
163 were intercrossed and the disrupted allele fixed to homozygosity. The new stock, formally
164 designated NOD/ShiLtDvs-*Nfkbid*$^{<em3Dvs>/}$Dvs (abbreviated as NOD-*Nfkbid*$^{-/-}$), was maintained
165 by brother-sister matting.

166 Previous reports indicated that *Nfkbid* deficient mice have an altered Foxp3^{+} Treg
167 compartment (31). Thus, we introduced the *Foxp3*$^{tm2(eGFP)-Tch}$ reporter construct previously
168 congenically transferred to the NOD strain (24) into the NOD-*Nfkbid*$^{-/-}$ stock and subsequently
169 fixed to homozygosity.
170
171 *Gene expression analysis*
172 Total RNA from whole thymus or sorted cell lysates was extracted using the RNeasy
173 mini kit (Qiagen, Germantown, MD, USA) following the vendor instructions. For whole thymus
174 tissue RNA, the complete organ was put in 2 ml of RNAlater stabilization solution (Thermo
175 Fisher Scientific, Waltham, MA, USA), incubated 24 h at room temperature and then stored at -
176 20˚C until processing. For RNA extraction from sorted cells, 2x10^{5} cells were sorted in 100%
177 FBS, washed 2 times in cold PBS and resuspended in RLT lysis buffer (Qiagen, Germantown,
178 MD, USA) and stored at -20˚C until processing. Extracted total RNA was quantified by
179 NanoDrop (Thermo Fisher Scientific, Waltham, MA, USA) and quality assessed in Bioanalyzer
180 (Agilent Technologies, Santa Clara, CA, USA). Samples with a RNA integrity index (RIN
181 index) of 7 or higher were used for gene expression analyses. For cDNA synthesis 500 ng of
182 total RNA was diluted to 5 µl in DEPC treated water and mixed with 5 µl of SuperScript IV
183 VILO Master Mix (Thermo Fisher Scientific, Waltham, MA, USA) following vendor
184 instructions.
185 Expression of *Nfkbid* was assessed by a predesigned and validated TaqMan qPCR assay
186 using Mm.PT.58.12759232 (IDT Integrated Technologies, Coralville, Iowa, USA) targeting the
187 exon 3-4 region and able to identify all four possible transcripts. The assay consists of a FAM-
188 labeled and double-quenched probe (5'-/56-FAM-CCTGGTGAT-/ZEN/-

189 GGAGGACTCTCTGGAT-/3IABkFQ/-3') and the primers p1 (5'-
190 GACAGGGAAGGCTCAGGATA-3') and p2 (5'-GCTTCCTGACTCCTGATTTCTAC-3').
191 The assay was reconstituted in 500µl of TE buffer (10 mM Tris-HCl pH 8.0, 0.1 mM EDTA)
192 generating a 20x solution that yield a final 1x solution of 500 nM primers and 250 nM probe. As
193 an endogenous control we used a predesigned and validated TaqMan assay for *Gapdh* (ID:
194 Mm99999915_g1) (VIC-labeled) (Applied Biosystems -Thermo Fisher Scientific, Waltham,
195 MA, USA). The qPCR analysis was done in a multiplexing setting combining both *Nfkbid* and
196 *Gapdh* assays using IDT prime Gene expression 2x master mix (IDT Integrated Technologies,
197 Coralville, Iowa, USA) and 6 ng of cDNA template in a final volume of 10µl. The experiment
198 was run in a ViiA-7 real time PCR system (Thermo Fisher Scientific, Waltham, MA, USA) with
199 four technical and four biological replicates, using the following program: 2 min at 50 ˚C, 3 min
200 at 95˚C, and 40 cycles of 3 min at 95˚C, 1 min 60˚C. An internal calibration curve was included
201 for both *Nfkbid* and *Gapdh*. The efficiency of each TaqMan assay was calculated from their
202 respective standard curves using the application SC, while relative gene expression was
203 determined by the ddCt method using the application RQ both in Thermo Fisher Cloud Software,
204 Version 1.0 (Thermo Fisher Scientific, Waltham, MA, USA).
205
206 *Microarray analysis*
207 Three to five 5-week-old, NOD.LCMV and NOD.Ln82-LCMV female mice were
208 injected i.v. with 0.5 µg of gp33 or D^b binding control peptide. Two hours post-injection whole
209 thymus tissue was processed as described above for total RNA extraction. Total RNA samples
210 were hybridized to Affymetrix Mouse Gene 1.0 ST Arrays. Average signal intensities for each
211 probe set within arrays were calculated by and exported from Affymetrix's Expression Console

212 (Version 1.1) software using the RMA method which incorporates convolution background
213 correction, summarization based on a multi-array model fit robustly using the median polish
214 algorithm, and sketch-quantile normalization. For this experiment, two pairwise comparisons
215 were used to statistically resolve gene expression differences between experimental groups using
216 the R/maanova analysis package (32). Specifically, differentially expressed genes were detected
217 by using F1, the classical F-statistic that only uses data from individual genes. Statistical
218 significance levels of the pairwise comparisons were calculated by permutation analysis (1000
219 permutations) and adjusted for multiple testing using the false discovery rate (FDR), q-value,
220 method (33). Differentially expressed genes are declared at an FDR q-value threshold of 0.05.
221 Two contrast groups were established: control D^b peptide (NOD.LCMV vs NOD.Ln82-LCMV),
222 and gp33 peptide (NOD.LCMV vs NOD.Ln82-LCMV). Data sets for contrast group Db and
223 gp33 were analyzed in IPA analysis software QIAGEN Bioinformatics (Redwood City, CA,
224 USA). Data were filtered for a expression fold change (EFC) > 2 and an expression FDR (q-
225 value) < 0.05.
226
227 *Flow cytometry analysis*
228 Single cell suspensions of thymus (Thy), spleen (SPL) and pancreatic lymph nodes
229 (PLN) from 5-6 week old female mice were prepared. Red blood cells in splenocytes samples
230 were lysed with Gey's buffer. $2x10^6$ cells were stained with the following monoclonal
231 antibodies: CD4-BV650 (GK1.5), CD8-PE-Cy7 (53-6.72), TCRVα8.3-FITC or PE (B21.14),
232 TCRVβ2-A647 (B20.6), TCRVβ8.1,2,3-FITC (F23.1) CD19-A700 (ID3), CD11b-PB (M1/70),
233 CD11c-PB (N418), CD21-FITC (7G6), CD23-PE (B3B4), CD5-PE (53-7.313) acquired from
234 BD Bioscience (San Jose, CA, USA) or BioLegend (San Diego, CA, USA), MHC class I

235 tetramers Tet-AI4-PE (H-2D^b/MimA2, sequence YAIENYLEL) (34) and Tet-NRPv7-PE (H-
236 2K^d/NRPv7) were acquired from the National Institutes of Health tetramer core facility (Atlanta,
237 GA, USA). Dead cells were excluded by DAPI staining. Stained cells were acquired using a
238 FACS LSRII instrument (BD Bioscience). All flow cytometric data were analyzed with FlowJo
239 (FlowJo LLC, Ashland, OR, USA).
240
241 *T-cell Proliferation assay*
242 Total splenic T-cells were purified from 5-week-old NOD and NOD-*Nfkbid*$^{-/-}$ female
243 mice by negative depletion of CD11c$^+$, CD11b$^+$, B220$^+$, Ter19$^+$, CD49b$^+$ cells with biotin-
244 conjugated antibodies and streptavidin magnetic beads over MACS columns (Miltenyi Biotech)
245 following manufacturer's protocols. Purified T-cells were washed with cold PBS, counted and
246 adjusted to a concentration of 2x10^7/ml for labeling with 10 μM cell tracer eFluor670
247 (eBioscience). Labeled cells were adjusted to 4x10^6/ml. Whole collagenase digested splenocytes
248 from NOD.*scid* mice were used as APCs. Labeled T-cells were seeded into a 96 well plate at a
249 density of 2x10^5/well with 4x10^5 APC/well in triplicate. Anti-CD3 monoclonal antibody (145-
250 2C11) was added at final concentrations of 4, 2, 1, 0.5, 0.25 and 0.125 μg/ml. The cells were
251 incubated at 37˚C, 5% CO_2 for 48h. T-cell proliferation was assessed by flow cytometric analysis
252 of cell tracer eFluor670 dilution. Proliferation parameters were obtained using the proliferation
253 platform analysis in FlowJo (FlowJo LLC, Ashland, OR, USA).
254
255 *Cytokine secretion analysis*
256 IL-2 and IFN-γ secretion was assessed in supernatants of T-cell proliferation cultures by
257 ELISA using BD OptEIA kits (BD Bioscience, San Diego, CA, USA).

258

259 *Western blot*

260 Whole thymus lysates were prepared in RIPA buffer (Cell signaling Technologies)
261 containing Halt protease inhibitor cocktail (Thermo Fisher Scientific). Total protein content was
262 quantified by Bradford assay (Thermo Fisher Scientific). 20µg of total protein were separated by
263 SDS-PAGE using Miniprotean TGX precast gradient 4-15% gels (Bio-rad Laboratories).
264 Proteins were electrotransferred to a PVDF membrane and incubated in blocking buffer (5%
265 Milk, TBST) overnight at 4˚C. The membrane was probed with a polyclonal rabbit anti-NFkbid
266 (35), , diluted at 1/1000 in 0.5% Milk/TBST, and incubated 1 hr at room temperature. Anti-
267 Rabbit-HRP diluted at 1/40000 in 0.5% Milk/TBST, was used as secondary Ab. Supersignal
268 Wes-fempto (Thermo Fisher Scientific) was used for chemiluminescent detection. β-Actin was
269 detected as loading control, over the same membrane after stripping, using mouse mAb anti-β-
270 Actin, and anti-mouse IgG-HRP.

271

272 *Diabetes incidence*

273 Diabetes was monitored once a week using urine glucose strips (Diastix, Bayer). Mice
274 with two consecutive readings >250mg/dl (corresponding to a blood glucose of >300mg/dl) were
275 considered diabetic.

276

277 *Statistical analysis*

278 Data analysis and graphs were made using Prism 6 software (GraphPad, San Diego, CA,
279 USA). Statistical analysis is detailed in the correspondent Figure Legends.

280

281 **Results**

282 *Mapping an Idd7 region gene(s) regulating thymic numbers of diabetogenic AI4 CD8$^+$ T-*
283 *cells to a 5.4 Mb region on Chr. 7.*

284 We previously developed a mouse stock, designated NOD.*Chr7^{B6}*FL-AI4, expressing the
285 transgenic AI4 TCR and congenic for a C57BL/6-derived segment of Chr.7 overlapping the
286 previously identified *Idd7* locus delineated by the flanking markers *Gpi1^b* (34.2 Mb) and
287 *D7Mit346* (58.7Mb) (29). AI4 T-cells underwent significantly higher levels of thymic deletion
288 at the DP stage of development in the NOD.*Chr7^{B6}*FL-AI4 congenic stock than in full NOD
289 background mice (8). This indicated a gene(s) allelically varying between NOD and B6
290 background mice mapping within the *Idd7* locus overlapping congenic interval played a strong
291 role in the extent diabetogenic AI4 TCR transgenic CD8$^+$ T-cells underwent thymic deletion (8).
292 We were subsequently able to derive from the original NOD.*Chr7^{B6}*FL-AI4 stock two sub-
293 congenic lines designated NOD.Ln82-AI4 (markers *D7Mit117–D7Mit247*) and NOD.Ln16-AI4
294 (markers *D7Mit79–D7Mit247*) (Fig. 1A). Analyses by flow cytometry found that compared to
295 NOD-AI4 controls, the yield of DP AI4 thymocytes (identified by staining with the TCR Vα8.3
296 specific monoclonal antibody B21.14) (Fig. 1B) was significantly decreased in the NOD.Ln82-
297 AI4 sub-strain (Fig. 1C). In contrast, the yield of AI4 DP thymocytes in the NOD.Ln16-AI4
298 stock were similar to that in NOD-AI4 controls (Fig. 1B, C). These differences indicated a 5.4
299 Mb region on Chr.7 delineated by the markers *D7Mit117-D7Mit225* contains a polymorphic
300 gene(s) influencing the extent to which DP AI4 thymocytes undergo negative selection.
301 Expression levels of the clonotypic Vα8.3 TCR element was higher in the NOD.Ln82-AI4 stock
302 compared to NOD-AI4 controls (Fig. 1D), a trait previously observed in NOD.*Chr7^{B6}*FL-AI4
303 mice (8). These results indicated a gene(s) in the 5.4 Mb region on Chr. 7 between *D7Mit117*

304 and *D7Mit225* may modulate how efficiently AI4 T-cell undergo thymic deletion through
305 regulation of TCR expression levels (8).
306
307 *Nfkbid is the only differentially expressed Idd7 region gene in diabetogenic CD8$^+$ T-cells*
308 *undergoing low versus high levels of thymic deletion.*
309
310 Due to differing cellular composition, we did not feel it appropriate to utilize thymii from
311 NOD-AI4 and NOD.Ln82-AI4 mice to carry out initial mRNA transcript analyses to identify
312 genes potentially contributing to the differential negative selection efficiency of diabetogenic
313 CD8$^+$ T-cells in these strains. Instead, we reasoned a more appropriate platform to carry out
314 such analyses would be provided by a previously produced NOD background stock
315 transgenically expressing a TCR (Vα2/Vβ8) recognizing the H2-D^b class I restricted gp33
316 peptide (KAVYNFATM) derived from Lymphocytic Choriomeningitis Virus (LCMV) (26, 27).
317 The basis for choosing this NOD.LCMV stock was that LCMV reactive CD8$^+$ T-cells
318 developing in the thymus would not be under any thymic negative selection pressure until such
319 time their cognate antigen is exogenously introduced. We generated an additional NOD.LCMV
320 stock homozygous for the Ln82 congenic interval. NOD.LCMV and NOD.Ln82-LCMV mice
321 were injected i.v. with 0.5µg of the gp33 or an H2-D^b binding control peptide (ASNENMETM).
322 At 24 hours post-injection, we assessed the proportion of LCMV specific DP thymocytes (TCR
323 Vα2$^+$) remaining present in NOD.LCMV and NOD.Ln82-LCMV mice that had received the
324 gp33 peptide relative to control cohorts. A significantly greater proportion of gp33 reactive DP
325 thymocytes were deleted in NOD.Ln82-LCMV than NOD.LCMV mice (Fig. 2A). These results

326 further indicated a polymorphic gene(s) in the *Idd7* region regulates the sensitivity of DP
327 thymocytes to undergo antigen-induced deletion.

328 The LCMV TCR transgenic system provided an opportunity to compare the influence of
329 the *Idd7* region over the transcriptional profile of thymocytes undergoing different levels of
330 antigen-induced negative selection. Time-course experiments indicated that at 2 and 4 hours
331 post-injection with the cognate antigen or peptide control there was no significant reduction in
332 the number of $V\alpha2^+$ DP thymocytes (Supplemental Fig. 2). However, we hypothesized that at 2-
333 hour post-antigen injection, a differential gene expression profile may have already been induced
334 in NOD.LCMV and NOD.Ln82-LCMV thymocytes contributing to their subsequent low and
335 high level of deletion seen at 24 hours. Using cutoff criteria of a q value <0.05, and minimum
336 two fold strain variation, microarray-based mRNA profiling found 16 and 212 genes were
337 respectively differentially expressed in thymocytes from NOD.LCMV and NOD.Ln82-LCMV
338 mice injected with the D^b binding control or gp33 peptide (Fig. 2B). This included 12 genes that
339 were commonly differentially expressed in thymocytes from NOD.LCMV and NOD.Ln82-
340 LCMV mice treated with either the control or gp33 peptide (Fig. 2B). None of the genes
341 differentially expressed in thymocytes from NOD.LCMV and NOD.Ln82-LCMV mice treated
342 with the control peptide mapped to the earlier defined 5.4 Mb *Idd7* support interval (genomic
343 coordinates 7:29,926,306-35,345,930). Intriguingly, *Nfkbid* was the only gene mapping to this
344 5.4 Mb *Idd7* support interval that was differentially expressed in thymocytes from NOD.LCMV
345 and NOD.Ln82-LCMV mice treated with the gp33 peptide (Fig. 3C). *Nfkbid* was expressed at a
346 3.6 fold higher level in thymocytes from gp33 treated NOD.LCMV than NOD.Ln82-LCMV
347 mice (Fig. 3C). We also subsequently found by RT-qPCR analyses that *Nfkbid* is expressed at

348 ~2 fold higher levels in flow cytometrically sorted equalized numbers of DP thymocytes from
349 NOD-AI4 than NOD.Ln82-AI4 mice (Fig. 2D).

350 *Nfkbid* (aka IκBNS) encodes a non-conventional modulator of the transcription factor
351 NF-κB (20), and ironically was first discovered as a gene expressed in thymocytes undergoing
352 negative, but not positive selection (21). Depending on cell type and physiological context
353 NFkbid can either positively or negatively modulated NF-κB activity (20). Low to moderate
354 levels of NF-κB activity (primarily the p50/p65 heterodimeric form) reportedly inhibits thymic
355 negative selection of CD8 lineage destined T-cells (36). On the other hand, high NF-κB activity
356 levels can elicit thymic negative selection of $CD8^+$ T-cells (36). Thus, either negative or positive
357 Nfkbid-mediated modulation of NF-κB activity could potentially contribute to the extent
358 diabetogenic $CD8^+$ T-cells undergo thymic deletion. For this reason, the rest of the current study
359 focused on testing the hypothesis that the higher *Nfkbid* expression variant in NOD than B6 mice
360 contributes to the less efficient thymic deletion of diabetogenic CD8 T-cells in the former strain.

361

362 *Generation of NOD-Nfkbid deficient mice*

363 In order to test whether the higher relative to B6 *Nfkbid* expression variant in NOD mice
364 contributes to diminished thymic deletion of diabetogenic $CD8^+$ T-cells, we utilized a
365 CRISPR/Cas9 approach to ablate this gene. The mouse *Nfkbid* gene is located on Chr.7 (genomic
366 coordinates GRCm38.p5 7: 30,421,732-30,428,746 and NOD_ShiLtJ_V1 7:31068239-
367 31076307), and has four alternative transcripts, three of which generate the same protein (327
368 amino acids) with a forth representing a non-coding sequence (37). Based on the reference
369 sequence (NM_172142.3), *Nfkbid* consist of 11 exons, 9 of them protein coding, with the start
370 codon located at the end of exon 3 (Fig. 3A). We designed a single guide RNA (gRNA) (Fig.

371 3A) with the intention to disrupt the start codon in exon 3 and thus eliminate translation of all
372 potential transcripts. We identified via PCR and targeted DNA sequencing a mutant line with a
373 deletion of 8 nucleotides including the start codon, and an additional Indel mutation consisting of
374 a 154 nucleotides copied from exon 2 and inserted in an inverted orientation in the Cas9 cutting
375 site (Fig. 3B). The mutation was fixed to homozygosity and the new stock was designated as
376 NOD-*Nfkbid*$^{-/-}$ (formally NOD/ShiLtDvs-*Nfkbid*$^{<emDvs3>}$/Dvs. Analyses of gene expression by
377 RT-qPCR indicated an absence of thymic *Nfkbid* transcript expression in NOD-*Nfkbid*$^{-/-}$ mice
378 compared to the easily detectable levels in wild type NOD controls (Fig. 3C). We performed
379 western blot analyses using total thymus lysates from NOD, NOD-*Nfkbid*$^{-/-}$, and B6.*Nfkbid*$^{-/-}$
380 mice (22, 31). Nfkbid was absent in both NOD and B6 Nfkbid deficient mice, while it was
381 present in wild type NOD mice (Fig. 3D).
382
383 *Diminution of Nfkbid expression enhances thymic deletion of both AI4 and NY8.3*
384 *diabetogenic CD8^{+} T-cells in NOD mice.*
385 We next evaluated whether diminution of *Nfkbid* expression enhanced the thymic
386 deletion of diabetogenic CD8^{+} T-cells in NOD mice. To initially do this, the inactivated *Nfkbid*
387 gene was transferred in both a heterozygous and homozygous state to the NOD-AI4 strain. As
388 expected analysis of gene expression by qPCR showed respective high and absent *Nfkbid* mRNA
389 transcript levels in thymocytes from NOD-AI4 and NOD-AI4-Nfkbid$^{-/-}$ mice (Fig. 4A). Also as
390 expected, *Nfkbid* mRNA transcript levels were significantly higher in thymocytes from NOD-
391 AI4 than B6.*H2*^{g7} control mice (Fig. 4A). A finding of potential physiological relevance was that
392 thymic *Nfkbid* mRNA transcript expression in NOD-AI4-Nfkbid$^{+/-}$ heterozygous mice was
393 reduced to a level not differing from B6.*H2*^{g7} controls (Fig. 4A). Numbers of DP, but not CD8^{+}

394 SP thymocytes positively staining with the H2-D^b/MimA2 tetramer capable of binding the AI4
395 TCR (Tet-AI4) (gating strategy shown in Fig. 4B) were significantly less in both heterozygous
396 and homozygous *Nfkbid* knockout mice, compared to gene intact controls (Fig. 4C). The same
397 result was obtained by staining with Vα8.3 and Vβ2 specific antibodies binding the AI4 TCR
398 (results not shown). As shown in Fig. 1D, TCR expression was significantly higher on DP
399 thymocytes from NOD.$Ch7^{B6}$Ln82-AI4 congenic mice than in controls in which the *Idd7* region
400 was of NOD origin. In contrast, partial or complete ablation of *Nfkbid* did not alter AI4 TCR
401 expression levels on either DP or $CD8^+$ SP thymocytes (Fig. 4D). Thus, some *Idd7* region
402 gene(s) other than *Nfkbid* regulates thymic TCR expression levels. These results also disprove
403 an earlier hypothesis (8) that an *Idd7* region gene(s) may control the thymic deletion efficiency
404 of diabetogenic $CD8^+$ T-cell by modulating TCR expression levels.

405 We next tested whether the apparent ability of varying *Nfkbid* expression levels to
406 modulate the thymic deletion efficiency of diabetogenic $CD8^+$ T-cells extended to clonotypes
407 beyond AI4. Thus, we introduced the *Nfkbid* knockout allele into a NOD stock with $CD8^+$ T-
408 cells transgenically expressing the NY8.3 TCR (NOD.NY8.3) that recognizes a peptide derived
409 from the ß-cell protein islet-specific glucose-6-phosphatase catalytic subunit-related protein
410 (IGRP) (28, 38). As observed for the AI4 clonotype, numbers of DP thymocytes staining with a
411 tetramer (designated NRPV7) recognized by the NY8.3 TCR (Fig. 5A) were significantly less in
412 6-week-old NOD.NY8.3-$Nfkbid^{+/-}$ heterozygous mice than in controls (Fig. 5B). When examined
413 at 4 weeks of age, numbers of both NY8.3 DP and $CD8^+$ SP thymocytes were significantly less
414 in NOD.NY8.3-$Nfkbid^{-/-}$ homozygous mice than in controls (Fig. 5C). Also, similar to the case
415 observed for the AI4 clonotype, expression levels of the NY8.3 TCR on DP or $CD8^+$ SP
416 thymocytes was not altered by the presence or absence of Nfkbid (Fig. 5D). Thus, based on

417 assessments of two separate clonotypes we conclude the *Nfkbid* expression variant characterizing
418 NOD mice represents the *Idd7* region gene contributing to impaired thymic deletion of
419 diabetogenic $CD8^+$ T-cells in this strain.
420
421 *Nfkbid deficiency paradoxically contributes to accelerated T1D in NOD mice by*
422 *impairing development of regulatory lymphocyte populations.*
423 We previously found that *Idd7* region gene effects were restricted to the thymus. This
424 was based on findings that while numerically reduced in the thymus, the AI4 T-cells that did
425 reach the periphery of B6.$H2^{g7}$ and NOD.$Ch7^{B6}$FL background mice were still able to expand
426 and mediate T1D development (7). However, we were surprised to find T1D development was
427 actually accelerated in NOD-*Nfkbid*$^{-/-}$ mice (Fig. 6A). This prompted us to assess if ablation of
428 the *Nfkbid* gene in NOD mice induced any numerical or functional differences in peripheral
429 leukocyte populations varying from those previously reported in B6 mice carrying a similar
430 mutation, but that exhibited no signs of autoimmunity (22, 31, 39). As previously observed for
431 the B6 background stock, numbers of splenic $CD4^+$ and $CD8^+$ T cells in NOD-*Nfkbid*$^{-/-}$ mice did
432 not differ from wild type controls (data not shown). As previously observed in B6 (40), marginal
433 zone (MZ) B-lymphocytes in the spleen and B1a cells in the peritoneum were both significantly
434 reduced in *Nfkbid* deficient NOD mice (Fig. 6B, C). The proliferative capacity of $CD4^+$ and
435 $CD8^+$ T-cells and their ability to secrete the cytokines IL-2 and IFNγ was reported to be
436 diminished in *Nfkbid* deficient B6 mice (22). Similar phenotypes characterized $CD4^+$ and $CD8^+$
437 T-cells from NOD-*Nfkbid*$^{-/-}$ mice (Fig. 6D, E). Ablation of *Nfkbid* has also been reported to
438 diminish numbers of FoxP3 expressing Tregs in B6 background mice (31). A similar effect was
439 elicited by ablation of *Nfkbid* in the NOD strain (Fig. 6F). Previous reports indicates that Nfkbid

440 is a direct regulator of IL-10 (35). We found that proportions of FoxP3^{+} and FoxP3^{-} CD4^{+} T-cells
441 producing immunosuppressive IL-10 upon *ex vivo* stimulation were significantly lower in *Nfkbid*
442 deficient than intact NOD mice (Fig. 6G). We recently found that partially overlapping
443 populations of CD73 expressing and IL-10 producing B-lymphocytes can mediate peripheral
444 regulatory effects (Bregs) inhibiting autoimmune T1D developments in NOD mice (41).
445 Ablation of *Nfkbid* also reduced levels of such IL-10 producing and CD73 expressing B-
446 lymphocytes in NOD mice (Fig. 6H, I). Thus, while diminishing *Nfkbid* expression enhances
447 thymic negative selection of diabetogenic CD8^{+} T cells in NOD mice, the coincidental decrease
448 in numbers of immunoregulatory lymphocyte populations likely accounts for why any
449 pathogenic effectors that do reach the periphery still aggressively induce disease development.
450
451
452
453
454
455

456 **Discussion**

457 It has become increasingly appreciated that in addition to the strong contributions
458 provided by some class II region genes, that when expressed in the proper genomic context,
459 particular common MHC class I variants are also key contributors to T1D development.
460 Previous work demonstrated primarily due to interactions with some non-MHC gene(s) in the
461 *Idd7* locus on proximal Chr. 7 the common class I variants expressed by NOD mice (K^d, D^b)
462 have a significantly lessened ability to mediate the thymic negative selection of diabetogenic
463 $CD8^+$ T-cells (7). In this study, through congenic truncation analyses we initially fine mapped
464 the *Idd7* region gene(s) controlling the efficiency of diabetogenic $CD8^+$ T-cell thymic deletion to
465 a 5.4 Mb interval on proximal Chr. 7. Identification of the responsible *Idd7* region gene was
466 greatly aided by the exploitation of NOD.LCMV TCR transgenic stocks that did or did not carry
467 a B6 derived congenic interval encompassing the relevant region of proximal Chr. 7. The
468 advantage of these stocks is that their thymocytes are under no negative selection pressure until
469 such time the LCMV cognate gp33 antigenic peptide is deliberately introduced. Upon
470 introduction of the gp33 peptide LCMV DP thymocytes were deleted to a significantly greater
471 extent in the presence of B6 rather than NOD derived genome across the relevant *Idd7* region.
472 Subsequent microarray based mRNA transcript analyses found following introduction of the
473 gp33 antigenic peptide *Nfkbid* was the only gene within the relevant 5.4 Mb region on Chr. 7 that
474 was differentially expressed in NOD.LCMV TCR mice carrying NOD or B6 genomic material
475 across the relevant *Idd7* region. The presence of NOD rather than B6 derived genome across this
476 *Idd7* region resulted in *Nfkbid* being expressed at 3-4 times higher levels in antigen stimulated
477 LCMV reactive thymocytes. This was similarly true for thymocytes transgenically expressing
478 the TCR from the naturally occurring diabetogenic AI4 $CD8^+$ T-cell clone derived from NOD

479 mice. Thus, we tested through CRISPR/Cas9 technology if diminishing or eliminating *Nfkbid*
480 expression in NOD mice resulted in improved thymic negative selection. NOD stocks in which
481 *Nfkbid* expression was either completely eliminated or reduced to B6-like levels were found to
482 have an improved capacity to mediate thymic negative selection of AI4 clonotypic cells as well
483 as those transgenically expressing the TCR from the diabetogenic NY8.3 $CD8^+$ T-cell clone.
484 These collective results indicated the higher *Nfkbid* expression variant in NOD than B6 mice is
485 likely the *Idd7* region gene strongly contributing to diminished thymic deletion of at least
486 diabetogenic $CD8^+$ T-cells in the former strain.

487 Nfkbid is mostly a nuclear protein formed by 7 ankyrin repeated domains (21). Due to the
488 lack of DNA binding and transactivation domains, Nfkbid function is mediated through protein-
489 protein interactions with NF-κB family members. Indeed Nfkbid can function as inhibitor or
490 enhancer of NF-κB activities depending on the protein partner and cell type (20). This includes
491 previously reported interactions of *Nfkbid* with the NF-κB subunit p50 (Nfkb1) in thymocytes
492 undergoing negative selection (21). However, our current results indicate *Nfkbid* is not required
493 for at least thymocytes destined for the $CD8^+$ lineage to undergo negative selection, and instead
494 its particular expression level in NOD mice appears to diminish the efficiency of this process.

495 Three different *Nfkbid* deficient mouse models have been previously produced, all on the
496 B6 background (22, 39, 42). These previously produced models have been useful to identify
497 several functional aspects of *Nfkbid*. In the B-cell compartment, *Nfkbid* expression is necessary
498 for development of the MZ and B1-a subsets as well as the generation of antibody responses to
499 T-dependent and independent antigens (22, 40, 42-44). *Nfkbid* deficiency was also associated
500 with an impairment in IL-10 secreting B-lymphocytes (45). *Nfkbid* deficient T-cells have

501 impaired *in vitro* proliferation and cytokine secretion (IL-2, IFN-γ) (22). We found these
502 phenotypes also characterize our *Nfkbid* deficient NOD mouse stock.

503 Interaction of Nfkbid with c-Rel has also been reported to contribute to Foxp3 expression
504 in Treg cells (31). Thus, we found it of interest that in addition to enhancing the thymic deletion
505 of diabetogenic $CD8^+$ T-cells, diminution of *Nfkbid* expression also resulted in decreased
506 numbers of peripheral Tregs in NOD mice. We recently reported that overlapping populations of
507 CD73 expressing and IL-10 producing B-lymphocytes can exert T1D protective
508 immunoregulatory activity in NOD mice (41). Ablation of *Nfkbid* expression also diminished
509 levels of both CD73 expressing and IL-10 producing B-lymphocytes in the periphery. Thus, we
510 conjecture it is the loss of both Tregs and these immunoregulatory B-lymphocytes that accounts
511 for the unexpected finding that T1D development is actually accelerated in *Nfkbid* deficient
512 NOD mice despite their improved, albeit not completely restored, ability to mediate the thymic
513 deletion of pathogenic $CD8^+$ T-cells. Hence, *Nfkbid* expression levels appears to act as a two-
514 edged sword, low levels in thymus can result in better negative selection of autoreactive $CD8^+$ T-
515 cells, but at the same time can contribute to autoimmunity in the periphery by diminishing levels
516 of regulatory lymphocyte populations.

517 In conclusion, *Nfkbid* appears to be an important contributory gene to how efficiently
518 autoreactive diabetogenic $CD8^+$ T-cells undergo thymic negative selection. However, this study
519 also revealed a caveat that would have to be considered if it might ultimately become possible to
520 diminish *Nfkbid* expression through pharmacological means. That is while diminishing *Nfkbid*
521 expression allows for increased thymic deletion of diabetogenic $CD8^+$ T-cells, it does so at the
522 price of decreasing levels of regulatory lymphocytes allowing any pathogenic effectors that do
523 reach the periphery to more rapidly induce disease onset. This explains our previous findings

524 that the *Idd7* region exerts two edged sword effects where the presence of B6 derived genome in
525 the region exerted T1D protective effects at the thymic level, but in the periphery actually
526 promotes disease development (8). Thus, when contemplating possible future interventions
527 designed to diminish numbers of diabetogenic T-cells, a consideration that should be taken into
528 account is whether the treatment might also impair regulatory cell numbers or activity allowing
529 the pathogenic effectors which do remain present to become more aggressive.

Acknowledgements

We would like to thank the Jackson Laboratory Research Animal Facility, Genetic Engineering Technology group, Flow Cytometry service, and Transgenic Genotyping core for technical support on this project. We thank the National Institutes of Health tetramer core facility for the tetramers used in this study.

Footnotes

[1] MP was supported by JDRF Fellowship 3-PDF-2014-219-A-N. For parts of this work, JJR1 was supported by either NIH Fellowship 1F32DK111078 or JDRF Fellowship 3-PDF-2017-372-A-N. He was also supported by a grant from the Diabetes Research Connection DRC 006887 JR. DVS is supported by NIH grants DK-46266, DK-95735, and OD-020351-5022. This work was also partly supported by Cancer Center Support Grant CA34196. The authors would also like to thank Carl Stiewe and his wife, Maike Rohde, for their generous donation toward T1D research at The Jackson Laboratory, which contributed to this work. IS was supported by grants of the Deutsche Forschunggemeinschaft (SCHM1586/6-1 and project A23 of SFB854)

[2] MP designed and conducted experimentation, interpreted data, and wrote the manuscript. JJR contributed to experimental design, data interpretation, and writing of the manuscript. JDL, JA and HDC conducted experimentation. JD and JR designed and conducted experiments and interpreted data. VKS and TS contributed to statistical analyses. YGC, AG and IS contributed to experimental design. DVS contributed to study conception, supervised experimental effort, and writing of the manuscript.

553 **References**

554

555 1. Atkinson, M. A., G. S. Eisenbarth, and A. W. Michels. 2014. Type 1 diabetes. *The*
556 *Lancet* 383: 69-82.
557 2. Ram, R., M. Mehta, Q. T. Nguyen, I. Larma, B. O. Boehm, F. Pociot, P. Concannon, and
558 G. Morahan. 2016. Systematic Evaluation of Genes and Genetic Variants Associated
559 with Type 1 Diabetes Susceptibility. *The Journal of Immunology* 196: 3043-3053.
560 3. Driver, J., D. Serreze, and Y.-G. Chen. 2011. Mouse models for the study of
561 autoimmune type 1 diabetes: a NOD to similarities and differences to human
562 disease. *Seminars in Immunopathology* 33: 67-87.
563 4. Geenen, V. 2012. Thymus and type 1 diabetes: an update. *Diabetes Res Clin Pract* 98:
564 26-32.
565 5. Jeker, L. T., H. Bour-Jordan, and J. A. Bluestone. 2012. Breakdown in Peripheral
566 Tolerance in Type 1 Diabetes in Mice and Humans. *Cold Spring Harbor Perspectives*
567 *in Medicine* 2.
568 6. Kishimoto, H., and J. Sprent. 2001. A defect in central tolerance in NOD mice. *Nat*
569 *Immunol* 2: 1025-1031.
570 7. Choisy-Rossi, C.-M., T. M. Holl, M. A. Pierce, H. D. Chapman, and D. V. Serreze. 2004.
571 Enhanced Pathogenicity of Diabetogenic T Cells Escaping a Non-MHC Gene-
572 Controlled Near Death Experience. *The Journal of Immunology* 173: 3791-3800.
573 8. Serreze, D. V., C. M. Choisy-Rossi, A. E. Grier, T. M. Holl, H. D. Chapman, J. R. Gahagan,
574 M. A. Osborne, W. Zhang, B. L. King, A. Brown, D. Roopenian, and M. P. Marron. 2008.
575 Through Regulation of TCR Expression Levels, an Idd7 Region Gene(s) Interactively
576 Contributes to the Impaired Thymic Deletion of Autoreactive Diabetogenic CD8+ T
577 Cells in Nonobese Diabetic Mice. *The Journal of Immunology* 180: 3250-3259.
578 9. von Boehmer, H., and F. Melchers. 2010. Checkpoints in lymphocyte development
579 and autoimmune disease. *Nat Immunol* 11: 14-20.
580 10. Klein, L., M. Hinterberger, G. Wirnsberger, and B. Kyewski. 2009. Antigen
581 presentation in the thymus for positive selection and central tolerance induction.
582 *Nat Rev Immunol* 9: 833-844.
583 11. Todd, J. A. 2010. Etiology of Type 1 Diabetes. *Immunity* 32: 457-467.
584 12. Pociot, F., B. Akolkar, P. Concannon, H. A. Erlich, C. Julier, G. Morahan, C. R. Nierras, J.
585 A. Todd, S. S. Rich, and J. Nerup. 2010. Genetics of Type 1 Diabetes: What's Next?
586 *Diabetes* 59: 1561-1571.
587 13. Drozina, G., J. Kohoutek, N. Jabrane-Ferrat, and B. M. Peterlin. 2005. Expression of
588 MHC II Genes. In *Molecular Analysis of B Lymphocyte Development and Activation*. H.
589 Singh, and R. Grosschedl, eds. Springer Berlin Heidelberg. 147-170.
590 14. Varanasi, V., L. Avanesyan, D. M. Schumann, and A. V. Chervonsky. 2012. Cytotoxic
591 Mechanisms Employed by Mouse T Cells to Destroy Pancreatic β-Cells. *Diabetes* 61:
592 2862-2870.
593 15. Knight, R. R., D. Kronenberg, M. Zhao, G. C. Huang, M. Eichmann, A. Bulek, L.
594 Wooldridge, D. K. Cole, A. K. Sewell, M. Peakman, and A. Skowera. 2013. Human β-
595 Cell Killing by Autoreactive Preproinsulin-Specific CD8 T Cells Is Predominantly

596 Granule-Mediated With the Potency Dependent Upon T-Cell Receptor Avidity.
597 *Diabetes* 62: 205-213.
598 16. Nejentsev, S., J. M. Howson, N. M. Walker, J. Szeszko, S. F. Field, H. E. Stevens, P.
599 Reynolds, M. Hardy, E. King, J. Masters, J. Hulme, L. M. Maier, D. Smyth, R. Bailey, J. D.
600 Cooper, G. Ribas, R. D. Campbell, D. G. Clayton, and J. A. Todd. 2007. Localization of
601 type 1 diabetes susceptibility to the MHC class I genes HLA-B and HLA-A. *Nature*
602 450: 887-892.
603 17. Noble, J. A., A. M. Valdes, M. D. Varney, J. A. Carlson, P. Moonsamy, A. L. Fear, J. A.
604 Lane, E. Lavant, R. Rappner, A. Louey, P. Concannon, J. C. Mychaleckyj, H. A. Erlich,
605 and f. t. T. D. G. Consortium. 2010. HLA Class I and Genetic Susceptibility to Type 1
606 Diabetes: Results From the Type 1 Diabetes Genetics Consortium. *Diabetes* 59:
607 2972-2979.
608 18. Ghosh, S., S. M. Palmer, N. R. Rodrigues, H. J. Cordell, C. M. Hearne, R. J. Cornall, J. B.
609 Prins, P. McShane, G. M. Lathrop, L. B. Peterson, and et al. 1993. Polygenic control of
610 autoimmune diabetes in nonobese diabetic mice. *Nat Genet* 4: 404-409.
611 19. McAleer, M. A., P. Reifsnyder, S. M. Palmer, M. Prochazka, J. M. Love, J. B. Copeman, E.
612 E. Powell, N. R. Rodrigues, J.-B. Prins, D. V. Serreze, N. H. DeLarato, L. S. Wicker, L. B.
613 Peterson, N. J. Schork, J. A. Todd, and E. H. Leiter. 1995. Crosses of NOD Mice With
614 the Related NON Strain: A Polygenic Model for IDDM. *Diabetes* 44: 1186-1195.
615 20. Schuster, M., M. Annemann, C. Plaza-Sirvent, and I. Schmitz. 2013. Atypical IkappaB
616 proteins - nuclear modulators of NF-kappaB signaling. *Cell Communication and*
617 *Signaling* 11: 23.
618 21. Fiorini, E., I. Schmitz, W. E. Marissen, S. L. Osborn, M. Touma, T. Sasada, P. A. Reche,
619 E. V. Tibaldi, R. E. Hussey, A. M. Kruisbeek, E. L. Reinherz, and L. K. Clayton. 2002.
620 Peptide-Induced Negative Selection of Thymocytes Activates Transcription of an NF-
621 kB Inhibitor. *Molecular cell* 9: 637-648.
622 22. Touma, M., V. Antonini, M. Kumar, S. L. Osborn, A. M. Bobenchik, D. B. Keskin, J. E.
623 Connolly, M. J. Grusby, E. L. Reinherz, and L. K. Clayton. 2007. Functional Role for
624 IκBNS in T Cell Cytokine Regulation As Revealed by Targeted Gene Disruption. *The*
625 *Journal of Immunology* 179: 1681-1692.
626 23. Haribhai, D., W. Lin, L. M. Relland, N. Truong, C. B. Williams, and T. A. Chatila. 2007.
627 Regulatory T cells dynamically control the primary immune response to foreign
628 antigen. *J Immunol* 178: 2961-2972.
629 24. Presa, M., Y.-G. Chen, A. E. Grier, E. H. Leiter, M. A. Brehm, D. L. Greiner, L. D. Shultz,
630 and D. V. Serreze. 2015. The Presence and Preferential Activation of Regulatory T
631 Cells Diminish Adoptive Transfer of Autoimmune Diabetes by Polyclonal Nonobese
632 Diabetic (NOD) T Cell Effectors into NSG versus NOD-scid Mice. *The Journal of*
633 *Immunology*.
634 25. Graser, R. T., T. P. DiLorenzo, F. Wang, G. J. Christianson, H. D. Chapman, D. C.
635 Roopenian, S. G. Nathenson, and D. V. Serreze. 2000. Identification of a CD8 T cell
636 that can independently mediate autoimmune diabetes development in the complete
637 absence of CD4 T cell helper functions. *J Immunol* 164: 3913-3918.
638 26. Pircher, H., K. Burki, R. Lang, H. Hengartner, and R. M. Zinkernagel. 1989. Tolerance
639 induction in double specific T-cell receptor transgenic mice varies with antigen.
640 *Nature* 342: 559-561.

641 27. Serreze, D. V., E. A. Johnson, H. D. Chapman, R. T. Graser, M. P. Marron, T. P.
642 DiLorenzo, P. Silveira, Y. Yoshimura, S. G. Nathenson, and S. Joyce. 2001.
643 Autoreactive Diabetogenic T-Cells in NOD Mice Can Efficiently Expand From a
644 Greatly Reduced Precursor Pool. *Diabetes* 50: 1992-2000.
645 28. Verdaguer, J., D. Schmidt, A. Amrani, B. Anderson, N. Averill, and P. Santamaria.
646 1997. Spontaneous Autoimmune Diabetes in Monoclonal T Cell Nonobese Diabetic
647 Mice. *The Journal of Experimental Medicine* 186: 1663-1676.
648 29. Chen, J., P. Reifsnyder, F. Scheuplein, W. Schott, M. Mileikovsky, S. Soodeen-
649 Karamath, A. Nagy, M. Dosch, J. Ellis, F. Koch-Nolte, and E. Leiter. 2005. "Agouti
650 NOD": identification of a CBA-derived Idd locus on Chromosome 7 and its use for
651 chimera production with NOD embryonic stem cells. *Mammalian Genome* 16: 775-
652 783.
653 30. Hill, J. T., B. L. Demarest, B. W. Bisgrove, Y.-C. Su, M. Smith, and H. J. Yost. 2014. Poly
654 peak parser: Method and software for identification of unknown indels using sanger
655 sequencing of polymerase chain reaction products. *Developmental Dynamics* 243:
656 1632-1636.
657 31. Schuster, M., R. Glauben, C. Plaza-Sirvent, L. Schreiber, M. Annemann, S. Floess,
658 Anja A. Kühl, Linda K. Clayton, T. Sparwasser, K. Schulze-Osthoff, K. Pfeffer, J. Huehn,
659 B. Siegmund, and I. Schmitz. 2012. IκBNS Protein Mediates Regulatory T Cell
660 Development via Induction of the Foxp3 Transcription Factor. *Immunity* 37: 998-
661 1008.
662 32. Wu, H., M. K. Kerr, X. Cui, and G. A. Churchill. 2003. MAANOVA: A Software Package
663 for the Analysis of Spotted cDNA Microarray Experiments. In *The Analysis of Gene*
664 *Expression Data: Methods and Software*. G. Parmigiani, E. S. Garrett, R. A. Irizarry, and
665 S. L. Zeger, eds. Springer New York, New York, NY. 313-341.
666 33. Storey, J. D. 2002. A direct approach to false discovery rates. *Journal of the Royal*
667 *Statistical Society: Series B (Statistical Methodology)* 64: 479-498.
668 34. Lieberman, S. M., T. Takaki, B. Han, P. Santamaria, D. V. Serreze, and T. P. DiLorenzo.
669 2004. Individual Nonobese Diabetic Mice Exhibit Unique Patterns of CD8+ T Cell
670 Reactivity to Three Islet Antigens, Including the Newly Identified Widely Expressed
671 Dystrophia Myotonica Kinase. *The Journal of Immunology* 173: 6727-6734.
672 35. Annemann, M., Z. Wang, C. Plaza-Sirvent, R. Glauben, M. Schuster, F. Ewald Sander, P.
673 Mamareli, A. A. Kühl, B. Siegmund, M. Lochner, and I. Schmitz. 2015. IκBNS Regulates
674 Murine Th17 Differentiation during Gut Inflammation and Infection. *The Journal of*
675 *Immunology* 194: 2888-2898.
676 36. Jimi, E., I. Strickland, R. E. Voll, M. Long, and S. Ghosh. 2008. Differential Role of the
677 Transcription Factor NF-κB in Selection and Survival of CD4+ and CD8+
678 Thymocytes. *Immunity* 29: 523-537.
679 37. Aken, B. L., S. Ayling, D. Barrell, L. Clarke, V. Curwen, S. Fairley, J. Fernandez Banet, K.
680 Billis, C. García Girón, T. Hourlier, K. Howe, A. Kähäri, F. Kokocinski, F. J. Martin, D. N.
681 Murphy, R. Nag, M. Ruffier, M. Schuster, Y. A. Tang, J.-H. Vogel, S. White, A. Zadissa, P.
682 Flicek, and S. M. J. Searle. 2016. The Ensembl gene annotation system. *Database*
683 2016: baw093-baw093.
684 38. Amrani, A., J. Verdaguer, P. Serra, S. Tafuro, R. Tan, and P. Santamaria. 2000.
685 Progression of autoimmune diabetes driven by avidity maturation of a T-cell
686 population. *Nature* 406: 739-742.

39. Kuwata, H., M. Matsumoto, K. Atarashi, H. Morishita, T. Hirotani, R. Koga, and K. Takeda. 2006. IκBNS Inhibits Induction of a Subset of Toll-like Receptor-Dependent Genes and Limits Inflammation. *Immunity* 24: 41-51.
40. Touma, M., D. B. Keskin, F. Shiroki, I. Saito, S. Koyasu, E. L. Reinherz, and L. K. Clayton. 2011. Impaired B Cell Development and Function in the Absence of IκBNS. *The Journal of Immunology* 187: 3942-3952.
41. Ratiu, J. J., J. J. Racine, M. G. Hasham, Q. Wang, J. A. Branca, H. D. Chapman, J. Zhu, N. Donghia, V. Philip, W. H. Schott, C. Wasserfall, M. A. Atkinson, K. D. Mills, C. M. Leeth, and D. V. Serreze. 2017. Genetic and Small Molecule Disruption of the AID/RAD51 Axis Similarly Protects Nonobese Diabetic Mice from Type 1 Diabetes through Expansion of Regulatory B Lymphocytes. *The Journal of Immunology*.
42. Arnold, C. N., E. Pirie, P. Dosenovic, G. M. McInerney, Y. Xia, N. Wang, X. Li, O. M. Siggs, G. B. Karlsson Hedestam, and B. Beutler. 2012. A forward genetic screen reveals roles for Nfkbid, Zeb1, and Ruvbl2 in humoral immunity. *Proceedings of the National Academy of Sciences* 109: 12286-12293.
43. Pedersen, G. K., M. Àdori, S. Khoenkhoen, P. Dosenovic, B. Beutler, and G. B. Karlsson Hedestam. 2014. B-1a transitional cells are phenotypically distinct and are lacking in mice deficient in IκBNS. *Proceedings of the National Academy of Sciences* 111: E4119-E4126.
44. Pedersen, G. K., M. Ádori, j. M. Stark, S. Khoenkhoen, C. Arnold, B. Beutler, and G. B. Karlsson Hedestam. 2016. Heterozygous mutation in IκBNS leads to reduced levels of natural IgM antibodies and impaired responses to T-independent type 2 antigens. *Frontiers in Immunology* 7.
45. Miura, M., N. Hasegawa, M. Noguchi, K. Sugimoto, and M. Touma. 2016. The atypical IκB protein IκBNS is important for Toll-like receptor-induced interleukin-10 production in B cells. *Immunology* 147: 453-463.

715 **Figures**

Figure 1

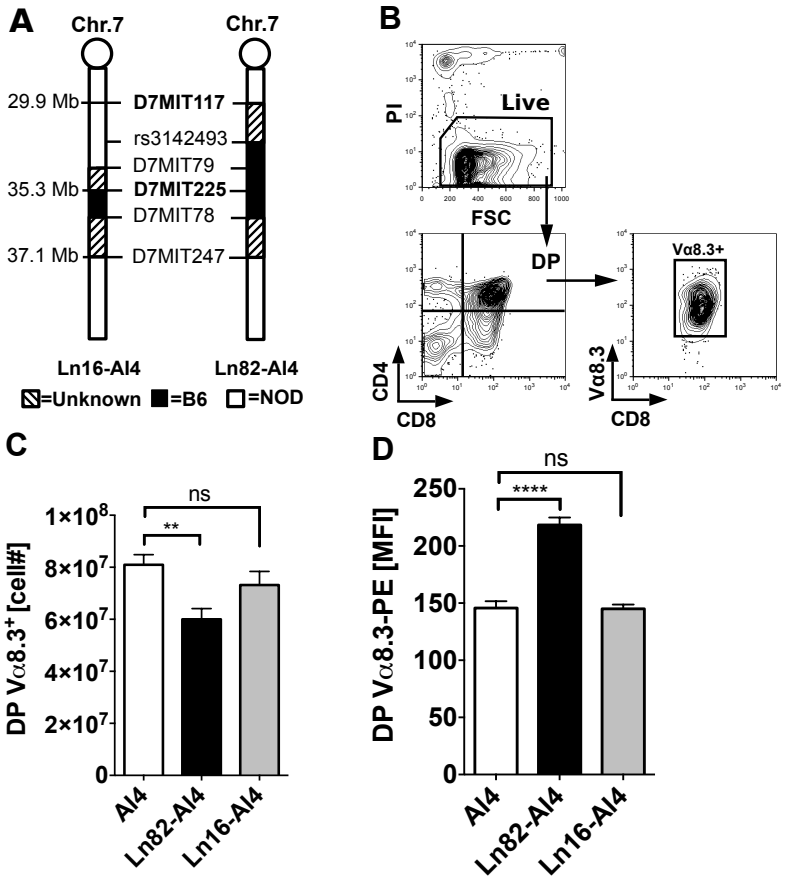

716

717 **Figure 1: Mapping an *Idd7* region gene(s) controlling the thymic negative selection**
718 **efficiency of diabetogenic AI4 CD8$^+$ T-cells to a 5.4 Mb region on Chr.7.** (**A**) Schematic
719 diagram of B6 derived Chr.7 congenic regions in NOD-AI4 mouse strains. Markers positions are
720 indicated in Mb based on genome assembly release GRCm38.p5 (37) (**B**) Flow cytometric gating
721 strategy to enumerate AI4 DP thymocytes. Thymocytes from 5-week-old female NOD-AI4
722 (n=32), NOD.Ln82-AI4 (n=20) and NOD.Ln16-AI4 (n=14) were stained with CD4, CD8 and
723 Vα8.3 specific antibodies. (**C**) Numbers of live (PI negative) CD4$^+$CD8$^+$ (DP) AI4 (Vα8.3$^+$)
724 thymocytes in the indicated strains. (**D**) Mean fluorescence intensity (MFI) of staining of DP
725 thymocytes from the indicated strains by the monoclonal antibody Vα8.3-PE. All values
726 represent mean±SEM of more than 3 independent experiments, statistical significance was
727 determined by Log-rank (Mantel-Cox) t-test (ns $p > 0.05$, ** $p < 0.001$, **** $p < 0.00001$).
728

729
730

Figure 2

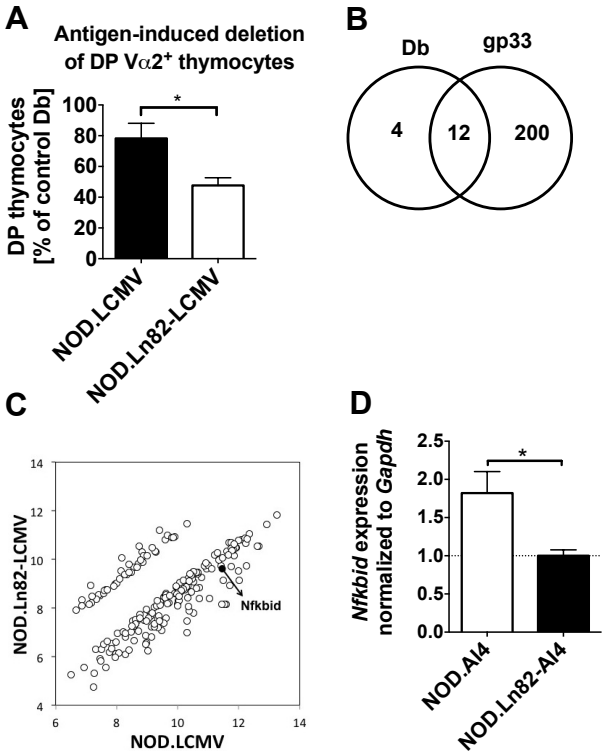

Figure 2: <u>*Nfkbid* is the only differentially expressed *Idd7* region gene in diabetogenic CD8$^+$ T-cells undergoing low versus high levels of thymic deletion</u>. (**A**) For antigen-induced negative selection, either 0.5 µg of gp33 (cognate antigen) or D^b binding control peptide were injected i.v. into five-week-old female NOD.LCMV (n=18 for controls and n=6 for gp33 treated) or NOD.Ln82-LCMV (n=22 for controls and n=6 for gp33 treated) mice. Remaining DP Vα2$^+$ thymocytes were quantified at 24 hours post-injection in each group. The efficiency of deletion was calculated as a ratio of the number DP Vα2$^+$ thymocytes remaining in gp33 treated mice to the average numbers in controls ($\frac{x\ gp33\ DP\ Va2+}{yDb\ DP\ Va2+} \times 100$) and expressed as a percentage. Statistical significance was determined by Log-rank (Mantel-cox) t-test (ns $p > 0.05$, * $p < 0.05$). (**B**) As assessed by microarray analyses number of genes deferentially expressed declared at a false discovery rate (q-value) <0.05 and a fold change ≥2 in thymocytes from NOD.LCMV and NOD.Ln82-LCMV 2 hours after i.v. injection with Db control or gp33 peptide. (**C**) Graph showing the average $\log_2$ (Intensity of probe set) for differentially expressed probe sets (same criteria as noted for panel B) between NOD.LCMV *vs* NOD.Ln82-LCMV mice injected i.v. two hours earlier with gp33 peptide. The arrow indicates *Nfkbid*. (**D**) Total RNA was extracted from $2x10^5$ DP Vß8$^+$ thymocytes sorted from 6-week-old female NOD.AI4 and NOD.Ln82-AI4 mice. *Nfkbid* mRNA relative quantification was done using the ddCt method and *Gapdh* as endogenous control and NOD.Ln82-AI4 mice as reference, mean relative fold change (RFC) ± SEM is indicated. * $p < 0.05$ unpaired t-test.

Figure 3

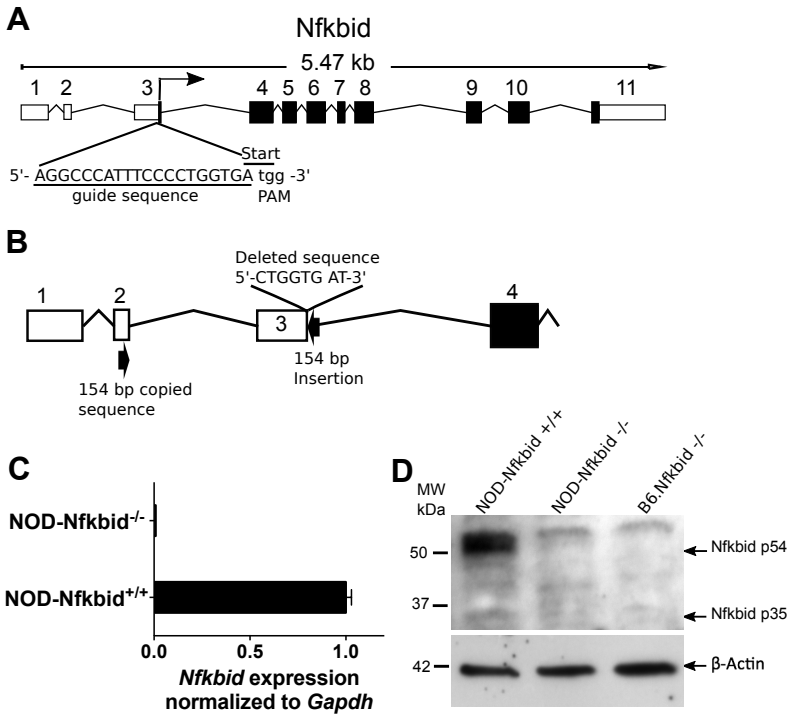

Figure 3: Targeting *Nfkbid* by CRISPR/Cas9 in NOD mice. (**A**) Representation of mouse *Nfkbid* gene showing the translation start site at the end of exon 3 and underlined the single guide RNA designed to target this region by CRISPR/Cas9. The PAM sequence is indicated in lower case.. (**B**) The resulting targeted mutation consisting of an 8 nucleotide deletion and an insertion of 154 nucleotides originated by copy and inversion of a segment from *Nfkbid* exon 2. (**C**) Total thymic RNA was extracted from NOD.*Nfkbid*$^{+/+}$ and NOD.*Nfkbid*$^{-/-}$ mice. Relative *Nfkbid* expression was analyzed by qPCR using *Gapdh* as endogenous control and NOD.*Nfkbid*$^{+/+}$ as a reference. Relative fold change (RFC) ± SEM is indicated. (**D**) Nfkbid protein expression was assessed by western blot analysis. Total thymus lysates from NOD, NOD.*Nfkbid*$^{-/-}$, and B6.*Nfkbid*$^{-/-}$ (negative control) were separated by SDS-PAGE and electro-transferred to a PVDF membrane. Nfkbid was detected using a previously validated polyclonal rabbit anti-Nfkbid. Nfkbid is detected as two isoforms, a 35 kDa and a high molecular weight of 54 kDa probably resulting from post-translational modifications. Lower panel indicates the detection of the loading control β-Actin obtained using the same membrane after stripping.

Figure 4

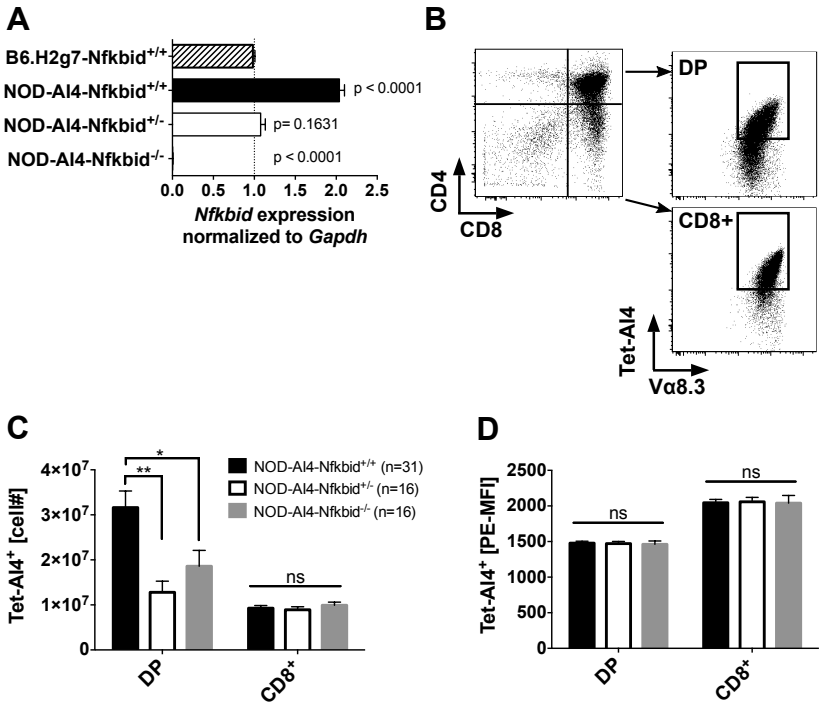

Figure 4: Genetic attenuation of *Nfkbid* expression controls the numbers of AI4 DP thymocytes. (**A**) *Nfkbid* gene expression was analyzed by qPCR of total thymus RNA from 6-week-old *B6.H2*^{g7} (n=2), NOD-AI4 (n=4), NOD-AI4-Nfkbid$^{+/-}$ (n=4) and NOD-AI4-Nfkbid$^{-/-}$ (n=3) mice. *Gapdh* was used as endogenous control and B6.*H2*^{g7} as the reference group. Graph shows the mean±SEM of relative fold change of *Nfkbid* expression normalized to *Gapdh*. Statistical significance was determined by one-way ANOVA and Bonferroni's multiple comparison test. The p-value of samples compared to the reference group is indicated. Note: We did not use B6.*H2*^{g7}-AI4 mice as a reference in this study because the numbers of thymocytes is extremely low and would not provide a fair comparison for gene expression analysis. (B) Illustration of gating to enumerate DP and CD8 SP thymocytes staining with the AI4 TCR specific tetramer. Depicted profiles are for thymocytes from a NOD-AI4 control. (C) Numbers of AI4 TCR expressing DP and CD8^{+} SP thymocytes from 6-week-old NOD-AI4, NOD-AI4-Nfkbid$^{+/-}$, and NOD-AI4-Nfkbid$^{-/-}$ female mice. Data represent the mean±SEM of DP or CD8^{+} SP thymocytes staining positive with the AI4 specific tetramer reagent. (D) Geometric MFI of AI4 tetramer staining of the same DP and CD8^{+} SP thymocytes evaluated in panel B. Bars represent the mean±SEM. Statistical significance was analyzed by 2-way ANOVA and Bonferroni's multiple comparison test. ns $p > 0.05$, * $p < 0.05$, ** $p < 0.01$.

Figure 5

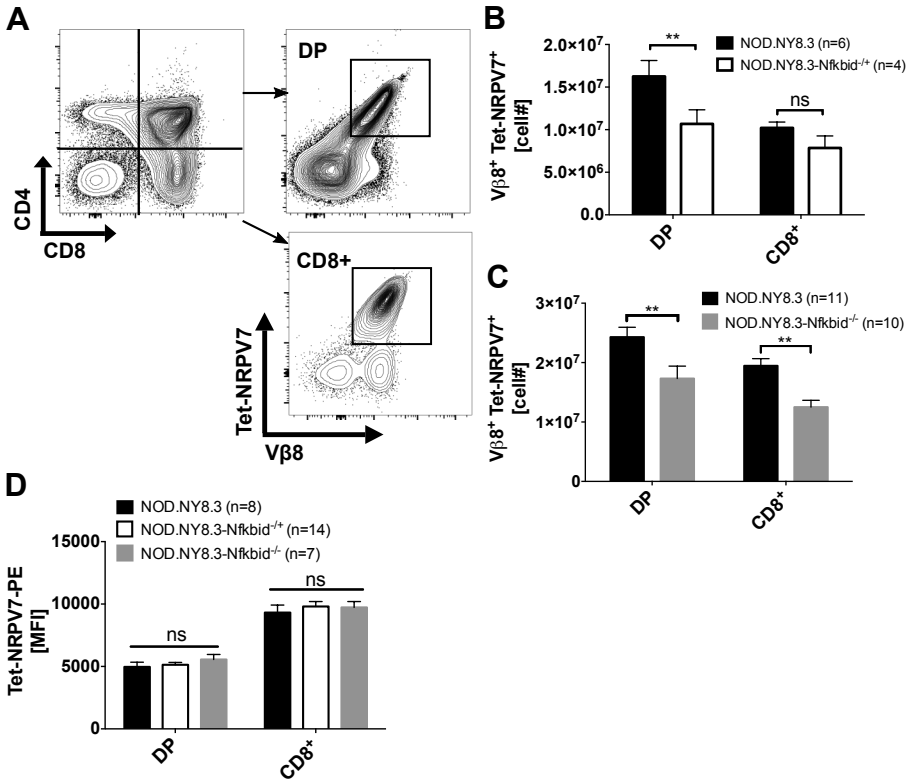

Figure 5: *Nfkbid* expression levels modulate thymic negative selection efficiency of diabetogenic NY8.3 clonotypic CD8$^+$ T-cells. (A) Illustration of gating to enumerate DP and CD8 thymocytes staining with the NY8.3 TCR specific NRPv7 tetramer. Depicted profiles are for thymocytes from a NOD.NY8.3 control. (B) Numbers of NY8.3 TCR expressing DP and CD8$^+$ thymocytes from 6-week-old female NOD.NY8.3 and NOD.NY8.3-*Nfkbid*$^{+/-}$ heterozygous mice. Data represent the mean±SEM of DP or CD8$^+$ SP thymocytes staining positive with the NY8.3 specific NRPv7 tetramer reagent. (C) Numbers of NY8.3 TCR expressing DP and CD8$^+$ SP thymocytes from 4-week-old female NOD.NY8.3 and NOD.NY8.3-*Nfkbid*$^{-/-}$ homozygous mice. Bars represent the mean±SEM of 3 independent experiments. (D) Geometric MFI of NY8.3 tetramer staining of DP and CD8$^+$ SP thymocytes from NOD.NY8.3, NOD.NY8.3-*Nfkbid*$^{+/-}$, and NOD.NY8.3-*Nfkbid*$^{-/-}$ mice. Bars represent mean±SEM. Statistical significance was analyzed by 2-way ANOVA and Bonferroni's multiple comparison test. ns $p > 0.05$, ** $p < 0.01$.

Figure 6

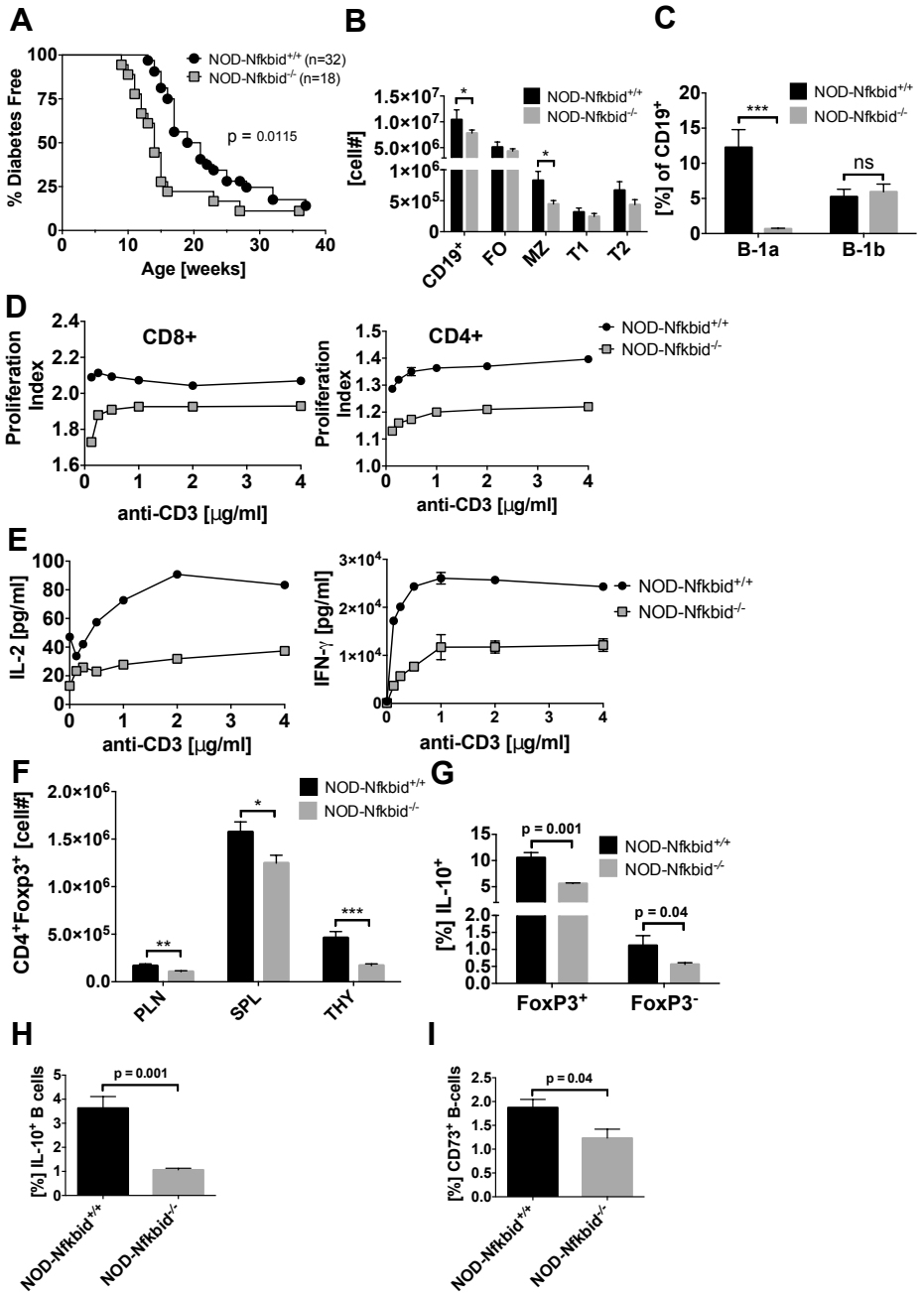

Figure 6: *Nfkbid* deficiency paradoxically accelerates T1D onset in NOD mice by impairing development of regulatory lymphocyte populations.
(A) T1D development was analyzed in a cohort of NOD and NOD.*Nfkbid*$^{-/-}$ female mice. Survival curve comparisons were analyzed through Log-rank (Mantel-Cox) test. (B) Splenocytes from 7 week old female NOD (n=3) and NOD.*Nfkbid*$^{-/-}$(n=5) mice were labeled with Ab for CD19, CD21 and CD23 and analyzed by flow cytometry. Singlet, DAPI^{-} CD19^{+} cells were identified as total B-cells. Based on expression of CD23 and CD21, B-cells were classified as follicular (FO: CD23^{+}CD21^{lo}), marginal zone (MZ: CD23^{-}CD21^{hi}) transitional 1 (T1: CD23^{-} CD21^{-}) and transitional 2 (T2: CD23^{int} CD21^{hi}) (C) Peritoneal cavity B-cells were isolated by

821 lavage with cold HBSS from the same group of mice described in (B), and stained for CD19,
822 B220, CD5 and analyzed by flow cytometry. Total B-cells (Singlet, DAPI^{-} CD19^{+}) were
823 classified based in the expression of B220 and CD5 as B1-a (CD5^{+} B220$^{int/lo}$) and B1-b (CD5^{-}
824 B220^{lo}) (D) The proliferation capacity of purified total T-cells from NOD and NOD.*Nfkbid*$^{-/-}$
825 mice was assessed as described in methods section. Briefly, MACS purified total T-cells were
826 labeled with cell tracer eFluor670 and stimulated *in vitro* with increasing amounts of anti-CD3
827 mAb. After 48 hours of culture the cells were labeled with Ab for CD4 and CD8. Proliferation
828 in CD4 and CD8 T-cell subsets was analyzed by flow cytometric analyses of cell tracer
829 eFluor670 dilution. Proliferation index was determined using the Flow Jo cell proliferation tool.
830 Data represent the mean±SEM of 3 technical replicates. (E) Cell culture supernatants of purified
831 T-cells used in the proliferation assay were assessed for secretion of the cytokines IL-2 and IFN-
832 γ by ELISA. Data represent mean±SEM of 3 technical replicates. (F) Enumeration of splenic
833 CD4^{+} FoxP3^{+} (based on *Foxp3*$^{tm2(eGFP)-Tch}$ reporter expression) Tregs in 6-week-old female NOD
834 (n=5) and NOD.*Nfkbid*$^{-/-}$ mice (n=9). (G) Analysis by intracellular staining and subsequent flow
835 cytometric analyses of proportion of Foxp3^{+} and FoxP3^{-} splenic CD4^{+} T-cells from 6-week-old
836 female NOD (n=5) and NOD.*Nfkbid*$^{-/-}$ mice (n=9) producing IL-10. (H) Analysis by intracellular
837 staining and subsequent flow cytometric analyses of proportions of IL-10 producing splenic B-
838 lymphocytes in 6-week-old female NOD (n=5) and NOD.*Nfkbid*$^{-/-}$ mice (n=9). (I) Proportions of
839 splenic CD73^{+} B-lymphocytes in 6-week-old female NOD (n=5) and NOD.*Nfkbid*$^{-/-}$ mice (n=9).
840 All bar graphs represent mean±SEM. Statistical significance was determined by 2-way ANOVA
841 and Bonferroni's multiple comparison test. ns $p > 0.05$, * $p < 0.05$, ** $p < 0.01$, *** $p < 0.001$.